applied sciences

MDPI

Article

Research on Non-Circular Raceway of Single-Row Four-Point Contact Ball Bearing Based on Life Optimization

Yanjie Zhao, Guanci Chen *, Wenbin Zhang and Yinke Ding

Faculty of Mechanical and Electrical Engineering, Kunming University of Science and Technology, Kunming 650500, China
* Correspondence: gcchen@kust.edu.cn

Abstract: The traditional slewing bearing with circular raceway has the problem of stress concentration under the large overturning moment. In this paper, a new non-circular raceway of a slewing ball bearing was presented to conquer this problem. To obtain the new non-circular raceway, first, the static equilibrium equations of the slewing ball bearing was established by the vector method, which is a constraint condition for life optimization; secondly, the life optimization function was established to calculate the contact load distribution in the bearing when the bearing life is at its maximum; finally, through the contact deformation with the contact load, the non-circular inner raceway corresponding to the maximum bearing life was obtained, and the non-circular shape corresponding to the raceway under axial load and overturning moment was studied. The results show that the non-circular raceway devised by this method can evenly reduce the contact force of the raceway and effectively improve the bearing capacity. Moreover, the position where the non-circular raceway deformation occurs is the position where the contact force is different before and after optimization. Therefore, the overturning moment has an effect on the shape of the raceway, whereas the axial load only affects the amplitude of the deformation, and has no obvious effect on the shape of the raceway.

Keywords: single-row four-point contact ball bearing; non-circular raceway; vector method; life optimization

check for updates

Citation: Zhao, Y.; Chen, G.; Zhang, W.; Ding, Y. Research on Non-Circular Raceway of Single-Row Four-Point Contact Ball Bearing Based on Life Optimization. *Appl. Sci.* **2022**, *12*, 13027. https://doi.org/10.3390/app122413027

Academic Editors: Hui Liu, Kai Long and Qi Xia

Received: 3 November 2022
Accepted: 15 December 2022
Published: 19 December 2022

Publisher's Note: MDPI stays neutral with regard to jurisdictional claims in published maps and institutional affiliations.

Copyright: © 2022 by the authors. Licensee MDPI, Basel, Switzerland. This article is an open access article distributed under the terms and conditions of the Creative Commons Attribution (CC BY) license (https://creativecommons.org/licenses/by/4.0/).

1. Introduction

A single-row four-point contact slewing ball bearing can simultaneously withstand axial force, radial force and overturning moment of the joint action, and is widely used in lifting, mining, wind turbine, medical and other mechanical rotary devices [1–3]. The bearing usually moves at low speed [4,5]. Due to the huge overturning moment, the load is often concentrated on the rolling body far away from the axis of the overturning moment [6,7], resulting in stress concentration, plastic deformation, and fatigue damage of the raceway, which seriously affect the bearing capacity of the slewing bearing and its service life.

Many scholars have carried out research on reducing raceway load and improving bearing capacity. Kabus [8] studied the topology optimization of a cylindrical roller bearing support structure to reduce the raceway contact load evenly. Hou Guanghui [9] studied the non-uniform preloading of bolts and topology optimization of a support structure to reduce the maximum contact load of the slewing bearing raceway. Mao Yuze et al. [10] studied the equivalent radial preload when the radial clearance of the equivalent cylindrical roller bearing is negative, and studied the load distribution law inside the cylindrical roller bearing under negative clearance. Yue Jidong et al. [11] analyzed the influence of ring deformation on the contact load between steel ball and raceway under negative clearance conditions, and calculated the friction torque of four-point contact ball bearing under no-load condition according to the law of conservation of energy. Xu Shaoren [12] established the mechanical equilibrium equation of the slewing bearing at no-load (only bearing the

inner ring gravity, along the axial direction), and studied the relationship between the internal contact force of the bearing and the negative clearance. Li Yunfeng et al. [13] studied the influence of clearance on the load distribution of a single-row four-point contact slewing ball bearing by static method. The research shows that the smaller clearance value is beneficial to improve the bearing capacity. Researchers [14–16] have studied the existence of radial clearance and the influence of the shape of rolling elements on the contact stress, and suggest that having radial negative clearance minimizes the mutation of maximum contact stress. Chen [17] established a nonlinear mechanical solution model to study the influence of different geometric parameters of the bearing on the bearing capacity. It was concluded that the axial clearance has an effect on the contact force, whereby it decreases with the decrease in axial clearance; when the clearance is close to 0, the contact force can be minimized and the bearing capacity can be effectively improved. The above scholars employed the method of uniformly reducing the contact load of the bearing. Compared with other traditional methods, the negative clearance can directly change the contact deformation of the rolling element and the raceway, which is better for uniformity and for reducing the contact load of the raceway. However, when the negative clearance is not selected properly, it increases the contact load of the raceway and the friction torque of the bearing. Moreover, the existing negative clearance method uses the same clearance in the circumferential direction of the slewing bearing, and does not give full play to the deformation control of the rolling element and the raceway.

In order to solve this problem, a new idea of designing a non-circular raceway for a slewing bearing is proposed in this paper, which is to uniformly reduce the contact load of the rolling element and improve the bearing capacity by precisely controlling the deformation of the raceway locally.

Scholars at home and abroad have done relevant research on non-circular deformation of bearing raceways. Rok Potocnik et al. [18,19] proposed a method based on vector representation to establish a static model of an arbitrary shape raceway of a four-point contact slewing ball bearing. The geometric deformation of the axial curvature center of the outer raceway of the bearing is defined by the sine wave function, and its influence on the static bearing capacity of a large double row slewing ball bearing has been studied. Wang [20] proposed a numerical method for determining the three-dimensional contact stress of cageless bearings, and studied the influence of a variable diameter bearing raceway on the contact characteristics between the rolling element and the raceway of cageless bearings and the bearing wear. Luo Tianyu et al. [21] studied the influence of outer raceway ellipticity on bearing life, and put forward the requirement of raceway ellipticity control. He Pingping [22] established a quasi-static model of an elliptical raceway of angular contact ball bearings under combined loads, studied the influence mechanism of the elliptical raceway on contact characteristics of the bearings, and estimated the fatigue life of bearings under elliptical raceway. Li Yunfeng [23] used the finite element method to analyze the deformation of the pitch bearing considering the installation structure. The results show that the inner ring of the wind turbine pitch bearing produces warping deformation in the axial plane and elliptical deformation in the radial plane. These deformations cause the load distribution curve of the steel ball to deviate from the sinusoidal distribution curve obtained under the traditional rigid ring assumption. The above scholars have studied the elliptical deformation in the radial plane and the warping deformation in the axial plane of the bearing raceway, and studied some effects of deformation on the mechanical properties of the bearing. However, their research mainly involves the small deformation of the raceway caused by the errors generated during the manufacturing and assembly of the bearing, and does not study the non-circular optimization of the initial raceway of the bearing and its influence on the load distribution of the raceway.

This paper takes a single-row four-point contact wind turbine slewing ball bearing as an example, establishes the static vector balance equation of the bearing under any raceway based on the Hertzian contact theory, uses the Newton iteration method to solve the balance equation, and studies the bearing inside the traditional circular raceway. Based

on the research results, the rated life of the bearing ring is calculated using the L-P theory, and the maximum life is used as the objective function to optimize the optimal non-circular deformation of the raceway corresponding to the maximum life of the bearing. The research on non-circular raceways of wind turbine slewing bearings will provide a new idea and method for improving the carrying capacity and life of small-angle slewing bearings, which can not only be used in wind turbine bearings, but also in lifting, mining, and medical treatment.

2. Static Equilibrium Equation of the Slewing Ball Bearing

Single-row four-point contact slewing ball bearings are elastomers with rolling elements as fulcrums. The machining errors of rolling elements and raceways and the stiffness of rings uniformly affect the internal load distribution and the change of contact angle. For the convenience of calculation, the following assumptions are made in the process of establishing and solving the mechanical model of a slewing bearing.

1. Both the inner and outer rings of the bearing are rigid, and elastic deformation occurs only at the contact point between the rolling element and the raceway.
2. The rolling element is a ball, its size has no deviation, the raceway is a pure circle, and there is no roundness error.
3. The material used for the ball and the rolling body is continuous without pores, the mechanical properties of all points inside the material are the same, and the mechanical properties of any point are the same in all directions.
4. The running speed of the slewing bearing is slow, and the influence of centrifugal force is ignored in the study.

2.1. Geometric Model

Figure 1 shows the sectional view of a single-row of four-point contact ball bearings. The z-axis is the axial direction of the bearing and the x-axis and y-axis are the radial direction of the bearing. Each ring of a four-point contact ball bearing consists of two arcs, each row of raceways having four arcs. Here, "inner upper" raceway is defined as the upper raceway arc of the inner ring; and "inner lower" raceway as the lower raceway arc of the inner ring. In like manner, "outer upper" raceway is defined as the upper raceway arc of the outer ring; and "outer lower" raceway as the lower raceway arc of the outer ring. The contact of the ball with "inner upper" and "outer lower" raceways forms contact pair 1, and the contact of the ball with "inner lower" and "outer upper" raceways forms contact pair 2. O_0 is the geometric center of the bearing, O is the center of the ball, D_{pw} is the pitch diameter of the bearing, D_w is the diameter of the ball, α_0 is the original contact angle of the bearing, g_0 is the clearance of the bearing, and id, iu stand for inner ring upper and lower raceway centers, and od, ou stand for outer ring upper and lower raceway centers, respectively.$o_{i,r}$, $o_{i,a}$, $o_{o,r}$, $o_{o,a}$ are the nominal radial and axial distances from the center of the rolling element to the center of the inner and outer raceways, respectively.

$$o_{i,r} = \left(r_i - \frac{D_w}{2}\right)\cos\psi \tag{1}$$

$$o_{i,a} = \left(r_i - \frac{D_w}{2}\right)\sin\psi \tag{2}$$

$$o_{o,r} = \left(r_o - \frac{D_w}{2}\right)\cos\psi \tag{3}$$

$$o_{o,a} = \left(r_o - \frac{D_w}{2}\right)\sin\psi \tag{4}$$

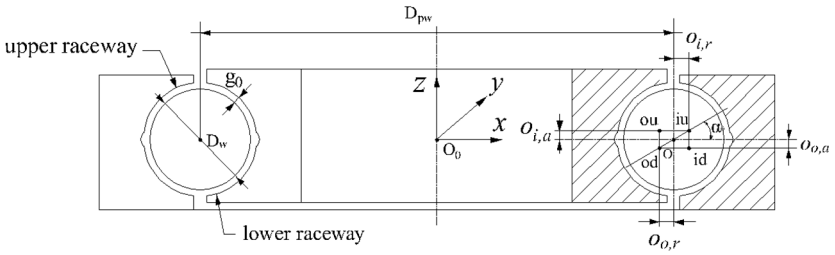


Figure 1. Sectional view of single-row four-point contact ball bearing.

In Equations (1)–(4), ψ is the azimuth angle of the bearing rolling element; r_i is the curvature radius of the inner raceway, and r_o is the curvature radius of the outer raceway—the value of which can be calculated according to the curvature coefficient of the inner and outer raceways and the diameter of the ball given by the bearing parameters [24].

Irregular bearing geometry is specified by the center of the irregularly shaped raceway [19]. The position relationship between the center of the bearing inner raceway and the center of the ball is shown in Figure 2. Based on the traditional circular raceway center, additional radial and axial displacements $\Delta_{i,r}$ and $\Delta_{i,a}$ are added to represent the arbitrary geometry of the inner raceway, where the additional displacement a is a function of the azimuth b of the rolling element, and the functional relationship between them can be obtained by other methods such as fitting. When a certain functional relationship is given, any reasonable geometry of the inner raceway of the bearing can be specified. The geometric shape of the outer raceway is the same, and the corresponding additional displacements are $\Delta_{o,r}$ and $\Delta_{o,a}$.

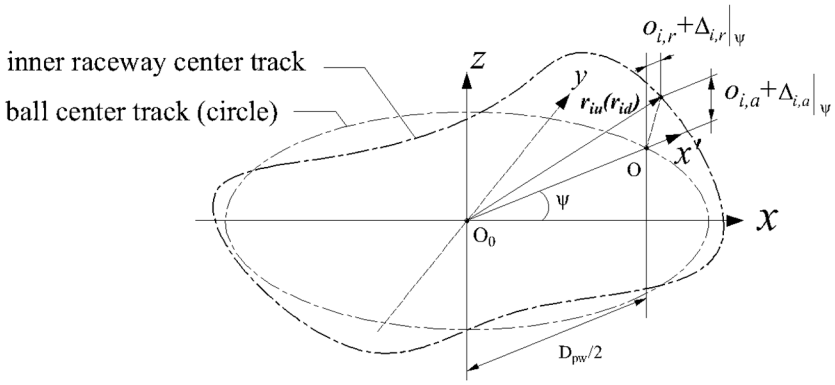


Figure 2. Irregular deformation of bearing inner raceway [19].

Therefore, the raceway center corresponding to any shape of the inner and outer rings of the bearing can be written as:

$$\vec{r_{iu}} = \vec{r_{ou}} = \begin{bmatrix} \left(\frac{D_{pw}}{2} \pm o_{i,r}\right)\cos\psi + \Delta_{i,r}|_\psi \\ \left(\frac{D_{pw}}{2} \pm o_{i,r}\right)\sin\psi + \Delta_{i,r}|_\psi \\ o_{i,a} + \Delta_{i,a}|_\psi \\ 1 \end{bmatrix} \tag{5}$$

$$\vec{r_{id}} = \vec{r_{od}} = \begin{bmatrix} \left(\frac{D_{pw}}{2} \pm o_{o,r}\right)\cos\psi + \Delta_{o,r}|_\psi \\ \left(\frac{D_{pw}}{2} \pm o_{o,r}\right)\sin\psi + \Delta_{o,r}|_\psi \\ -o_{o,a} + \Delta_{o,a}|_\psi \\ 1 \end{bmatrix} \tag{6}$$

where '+' (respectively '−') means that the calculated distance from the center point of the non-circular raceway to the bearing center O_0 is greater (respectively less) than the distance

from the center point of the circular raceway to the bearing center under the same azimuth angle (i.e., the radius of the bearing pitch circle).

Since we need to multiply the coordinate transformation matrix in the next section, the vector extends the fourth component, namely, the scalar 1.

2.2. Bearing Load State

Figure 3 shows the vector description of the bearing after loading. Among them, the bearing outer ring is fixed; and the loads on the inner ring, Q_1, Q_2 are the contact force between ball and raceway in the contact pairs 1 and 2, respectively.

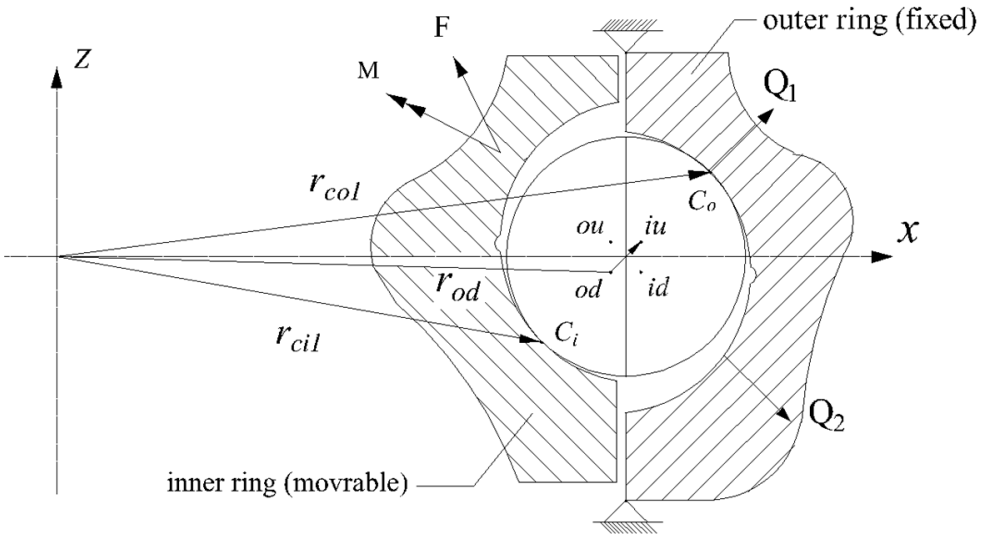


Figure 3. Vector description of load acting on bearing raceway.

Before the bearing is loaded, the curvature centers of the inner and outer raceways can be expressed as:

$$\vec{r_{iu}} = \vec{r_{ou}} = \begin{bmatrix} \left(\frac{D_{pw}}{2} \pm o_{i,r}\right)\cos\psi \\ \left(\frac{D_{pw}}{2} \pm o_{i,r}\right)\sin\psi \\ o_{i,a} \\ 1 \end{bmatrix} \tag{7}$$

$$\vec{r_{id}} = \vec{r_{od}} = \begin{bmatrix} \left(\frac{D_{pw}}{2} \pm o_{o,r}\right)\cos\psi \\ \left(\frac{D_{pw}}{2} \pm o_{o,r}\right)\sin\psi \\ -o_{o,a} \\ 1 \end{bmatrix} \tag{8}$$

After the bearing is loaded, under the action of axial force F_a, radial force F_r and overturning moment M, the displacements of the inner raceway relative to the outer raceway along the x-, y-, and z-axes are u, v, and w, respectively; and the deflection angles around the x- and y-axes are φ_x and φ_y, respectively. These movements can be given by the coordinate transformation matrix shown in Formula (9).

$$T = \begin{bmatrix} \cos\varphi_y & \sin\varphi_x\sin\varphi_y & \cos\varphi_x\sin\varphi_y & u \\ 0 & \cos\varphi_x & -\sin\varphi_x & v \\ -\sin\varphi_y & \cos\varphi_y\sin\varphi_x & \cos\varphi_x\cos\varphi_y & w \\ 0 & 0 & 0 & 1 \end{bmatrix} \tag{9}$$

Assuming that the deflection angle of the bearing due to load deformation is very small [17], where $\sin\varphi = \varphi$ and $\cos\varphi = 1$, the coordinate transformation matrix T can be simplified as follows:

$$T \approx \begin{bmatrix} 1 & \varphi_x\varphi_y & \varphi_y & u \\ 0 & 1 & -\varphi_x & v \\ -\varphi_y & \varphi_x & 1 & w \\ 0 & 0 & 0 & 1 \end{bmatrix} \tag{10}$$

The position of the curvature center after the inner raceway movement can be described as:

$$\vec{r_{iu,T}} = T \cdot \vec{r_{iu}} \vec{r_{id,T}} = T \cdot \vec{r_{id}} \tag{11}$$

After the inner raceway movement, the direction of contact force Q_1, Q_2 can be expressed by the unit vectors $e_{Q_1,T}$ and $e_{Q_2,T}$, respectively.

$$\vec{e_{Q_1,T}} = \frac{\vec{r_{iu,T}} - \vec{r_{od}}}{\left\| \vec{r_{iu,T}} - \vec{r_{od}} \right\|} \vec{e_{Q_2,T}} = \frac{\vec{r_{id,T}} - \vec{r_{ou}}}{\left\| \vec{r_{id,T}} - \vec{r_{ou}} \right\|} \tag{12}$$

Therefore, after the inner raceway movement, the action point of the contact force on the inner and outer raceways of the bearing can be calculated as:

$$Q_1 = \begin{cases} \vec{r_{c_o1}} = \vec{r_{od}} + \vec{e_{Q_1,T}} \cdot r_o \\ \vec{r_{c_i1,T}} = \vec{r_{iu}} - \vec{e_{Q_1,T}} \cdot r_i \end{cases} Q_2 = \begin{cases} \vec{r_{c_o2}} = \vec{r_{ou}} + \vec{e_{Q_2,T}} \cdot r_o \\ \vec{r_{c_i2,T}} = \vec{r_{id}} - \vec{e_{Q_2,T}} \cdot r_i \end{cases} \tag{13}$$

The size of the contact force depends on the contact deformation of the raceway and the rolling element. Therefore, the premise of calculating the contact force is to calculate the relative approach δ between the inner and outer raceways after bearing loading. Since the influence of bearing clearance is neglected in this paper, the initial relative approach degree is the rolling element diameter before bearing loading; after the bearing is loaded, the relative proximity a can be calculated as:

$$\delta_1 = D_w - \left\| \vec{r_{c_i1,T}} - \vec{r_{c_o1}} \right\| \delta_2 = D_w - \left\| \vec{r_{c_i2,T}} - \vec{r_{c_o2}} \right\| \tag{14}$$

When $\delta \leq 0$, it means that the distance between the two raceways after loading is greater than the diameter of the rolling element, that is, the ball and the raceway are not in contact. In this case, the contact force is 0. When $\delta > 0$, it means that there is contact stress between the rolling element and the raceway. The contact force can be expressed as:

$$Q = \begin{cases} K\delta^{3/2} & \delta > 0 \\ 0 & \delta \leq 0 \end{cases} \tag{15}$$

where K is the equivalent contact stiffness of the rolling element and raceway. Since this depends on the contact stiffness between the rolling element and the inner and outer raceways, the equivalent contact stiffness can be expressed as:

$$K = \left(\frac{1}{\left(\frac{1}{k_i}\right)^{2/3} + \left(\frac{1}{k_o}\right)^{2/3}} \right)^{3/2} \tag{16}$$

where k_i is the contact stiffness between the rolling element and the inner raceway, and k_o is the contact stiffness between the rolling element and the outer raceway. It depends on the material properties of the contact object and the geometric parameters of the contact body and can be calculated by Hertz contact theory [25].

Therefore, the equilibrium equation can be expressed as:

$$\sum_{j=1}^{Z}\left(Q_{1,j}\cdot\vec{e_{Q1,j}}+Q_{2,j}\cdot\vec{e_{Q2,j}}\right)=\vec{F} \tag{17}$$

$$\sum_{j=1}^{Z}\left(\vec{r_{c_o}1,j}\times\left(Q_{1,j}\cdot\vec{e_{Q1,j}}\right)+\vec{r_{c_o}2,j}\times\left(Q_{2,j}\cdot\vec{e_{Q2,j}}\right)\right)=\vec{M} \tag{18}$$

where Z is the number of balls.

Since the bearing rotates around the z-axis in actual operation, the torque balance along the z-axis is not considered. Thus, Equations (15) and (16) represent a system of five nonlinear equations with five unknown variables, i.e., displacements u, v, w and rotations φ_x and φ_y of the inner raceway. These variables are defined in the coordinate transformation matrix T, and when the corresponding external load is given, the distribution of the contact load inside the bearing can be obtained by the Newton-Raphson iteration method [26].

3. Maximum Life Optimization of Slewing Ball Bearing

3.1. Life Calculation Equations of Slewing Ball Bearing

Bearing life calculation conforms to L-P theory [27]. The bearings discussed in this paper are single-row four-point contact ball bearings. When calculating the rated life of the bearing, the following steps are required: first, the basic rated dynamic load of the bearing is calculated according to the model of the bearing. Secondly, the equivalent dynamic load of the corresponding contact of the four-point contact ball bearing on the upper and lower raceways is calculated according to the contact load obtained by the equilibrium equation; and the rated life of inner and outer rings of bearing are calculated, where the rated life of a single ring is the fitted value of two rings in contact with the steel ball. Finally, inner and outer raceway life are fitted to calculate the rated life of the bearing [28].

For four-point contact ball bearings, the basic rated dynamic load of the bearing ring is:

$$Q_{ci(o)j}=98.1\lambda\eta\left(\frac{2f_{i(o)}}{2f_{i(o)}-1}\right)^{0.41}\frac{(1\mp\gamma)^{1.39}}{(1\pm\gamma)^{1/3}}\cdot\left(\frac{D_w}{D_{pw}}\right)^{0.3}Z^{-1/3}3.624D_w^{1.4} \tag{19}$$

The sign above the formula is the rated dynamic load of the inner ring, and the sign below is that of the outer ring; f_i and f_o are the curvature coefficients of the inner and outer raceways of the bearing, λ, respectively; and η is the correction coefficient of the ball bearing, whose value can be found in [29].

In this article, the outer ring is fixed and the inner ring rotates, so the equivalent roller load on the inner raceway j is:

$$Q_{euj}=\left(\frac{1}{Z}\sum_{\psi=0}^{2\pi}Q_{j\psi}^3\right)^{1/3} \tag{20}$$

where $Q_{j\psi}$ is the rolling contact load, N.

The rated life of each raceway on the inner ring is:

$$L_{10ij}=\left(Q_{cij}\Big/Q_{e\mu j}\right)^3 \tag{21}$$

The rated life of the inner ring is:

$$L_{10i}=\left(\sum_{j=1}^{2}L_{10ij}^{-10/9}\right)^{-0.9} \tag{22}$$

The equivalent roller load on the outer ring raceway j is:

$$Q_{evj} = \left(\frac{1}{Z} \sum_{\psi=0}^{2\pi} Q_{j\psi}^{10/3} \right)^{0.3} \tag{23}$$

The rated life of each raceway on the outer ring is:

$$L_{10oj} = \left(Q_{coj} \Big/ Q_{evj} \right)^{3} \tag{24}$$

The outer ring rated life is:

$$L_{10o} = \left(\sum_{j=1}^{2} L_{10oj}^{-10/9} \right)^{-0.9} \tag{25}$$

The rated life of four-point contact ball bearings can be calculated as:

$$L_{10} = \left(L_{10i}^{-10/9} + L_{10o}^{-10/9} \right)^{-0.9} \tag{26}$$

3.2. Optimization Objective Function of Maximum Life

The relationship between the rated life of the bearing and the internal contact load is given in Equation (27). Taking the maximum rated life as the objective function, and the static equilibrium equation of the internal contact force of the bearing and the external load as the constraints, the distribution of the optimal contact force corresponding to the maximum rated life can be calculated as in [8]. The optimization is expressed as:

$$Maximize : L_{10}(Q) \tag{27}$$

This is subject to:

$$\sum_{j=1}^{Z} \left(Q_{1,j} \cos \alpha_{1,j} + Q_{2,j} \cos \alpha_{2,j} \right) \cos \psi_j = F_x \tag{28}$$

$$\sum_{j=1}^{Z} \left(Q_{1,j} \cos \alpha_{1,j} + Q_{2,j} \cos \alpha_{2,j} \right) \sin \psi_j = F_y \tag{29}$$

$$\sum_{j=1}^{Z} \left(Q_{1,j} \sin \alpha_{1,j} - Q_{2,j} \sin \alpha_{2,j} \right) = F_z \tag{30}$$

$$\sum_{j=1}^{Z} \left(Q_{1,j} \sin \alpha_{1,j} - Q_{2,j} \sin \alpha_{2,j} \right) \frac{D_{pw}}{2} \sin \psi_j = -M_x \tag{31}$$

$$\sum_{j=1}^{Z} \left(Q_{1,j} \sin \alpha_{1,j} - Q_{2,j} \sin \alpha_{2,j} \right) \frac{D_{pw}}{2} \cos \psi_j = M_y \tag{32}$$

where ψ_j is the position angle of each roller, and $\alpha_{1,j}$ and $\alpha_{2,j}$ are the angles between the contact force Q_1, Q_2 and the xy plane, respectively, which can be obtained from the geometric model. Since an external load is applied in five directions, the spatial stress component is considered in equilibrium. The distribution of contact force inside the bearing under maximum life can be obtained by solving Equations (28)–(32).

4. Method to Obtain the Non-Circular Inner Raceway

Figure 4 shows the offset distance of inner raceway, comparing it before and after bearing optimization. The outer raceway of the bearing is fixed, and the inner raceway is offset under load, where iu and iu' are the positions of curvature center of inner raceway before and after optimization. Therefore, the overall offset of the bearing after optimization is $\Delta = Oiu' - Oiu$, and from this, the axial ($\Delta_{i,a}$) and radial ($\Delta_{i,r}$) non-circular shapes before and after optimization can be obtained.

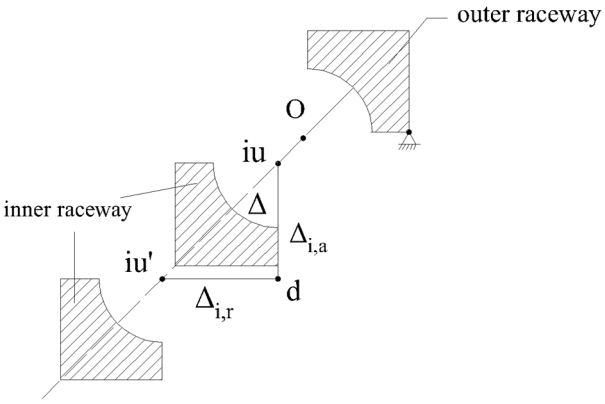


Figure 4. Comparison of bearing raceway movement before and after optimization.

Figure 5 shows the flow chart for solving non-circular raceway profiles.

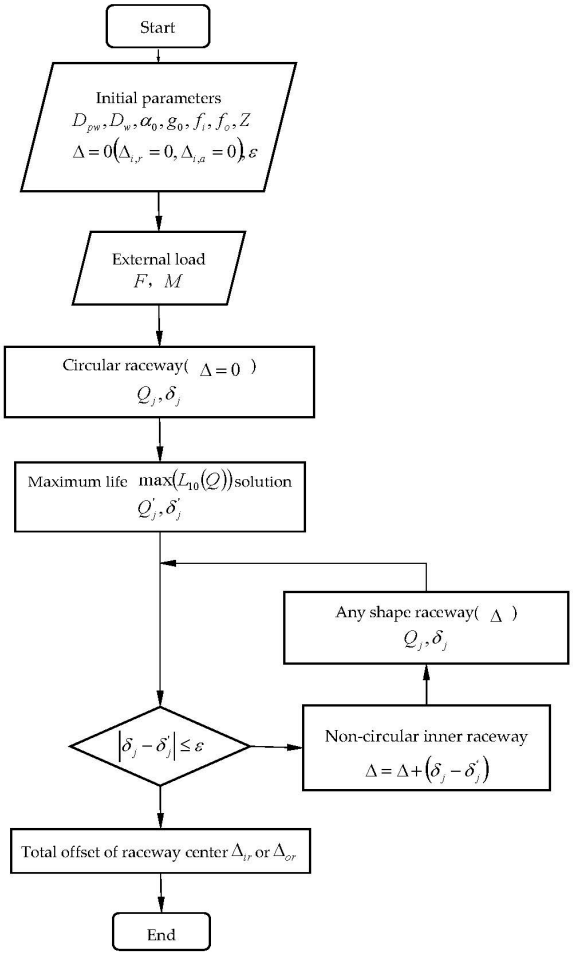


Figure 5. Non-circular raceway profile solving process.

First, the contact force Q and contact deformation δ_j under the circular raceway are calculated by the mechanical model, and then the corresponding contact force Q'_j and contact deformation δ'_j after life optimization are calculated; and the optimized contact deformation is taken as the criterion of convergence. Next, comparing δ_j and δ'_j: if the difference between the two is large, the shape of the raceway is adjusted by the difference $\Delta = \delta_j - \delta'_j$. After calculation and convergence, the total raceway offset is the final non-circular raceway profile parameter.

5. Results Analysis

The slewing bearing model used in this paper is the 787/434G2 single-row four-point contact ball bearing (toothless). The structural parameters are shown in Table 1, and the external load is shown in Table 2.

Table 1. Structural parameters of single-row four-point contact slewing ball bearing.

Parameter	Value
Ball diameter D_w (mm)	12.7
Bearing pitch diameter D_{pw} (mm)	545
Ball number Z	101
Nominal contact angle α_0 (°)	30
Inner raceway curvature coefficient f_i	0.54
Outer raceway curvature coefficient f_o	0.525
Clearance g_0 (mm)	0

Table 2. Maximum external loads for single-row four-point contact ball bearing.

Parameter	Value
$F_x(N)$	3000
$F_y(N)$	4000
$F_z(N)$	48,000
$M_x(N \cdot mm)$	−25,000,000
$M_y(N \cdot mm)$	35,000,000

5.1. Bearing Contact under Combined External Loads

5.1.1. Contact Load Distribution before and after Optimization

Figure 6a,b shows the bearing contact force distribution before and after optimization under the combined action of Table 2, where Q_{rigid} is the contact force before optimization and Q_{opt} is the optimized contact force. It can be seen from the figure that before optimization, the contact force Q_1 is greater than 0 in the range of azimuth 96.2–327.9°. The contact force Q_2 is greater than 0 in the ranges of 0–110.5° and 317.2–356.4°. The contact force Q_1 and Q_2 reach the maximum when the azimuth is 213.9° and 32.1° respectively (corresponding to 10,464 N and 10,492 N, respectively).

After optimization, the maximum values of contact force Q_1 and Q_2 decreased compared with those before optimization, resulting in Q_1 of 5410 N (decreased by 5054 N) and Q_2 of 4922 N (decreased by 5569 N). The azimuth angle corresponding to the maximum contact force did not change, remaining 213.9° and 32.1°, respectively. When the azimuth is 71.3–356.4°, the contact force Q_1 is greater than 0. When the azimuth angle is in the range of 0–131.9° and 303–356.4°, the contact force Q_2 is greater than 0. It can be deduced that compared with before optimization, the contact force inside the bearing is significantly reduced after optimization, and the bearing area of the rolling element is increased, which makes the rolling element load more uniform and effectively improves the bearing capacity.

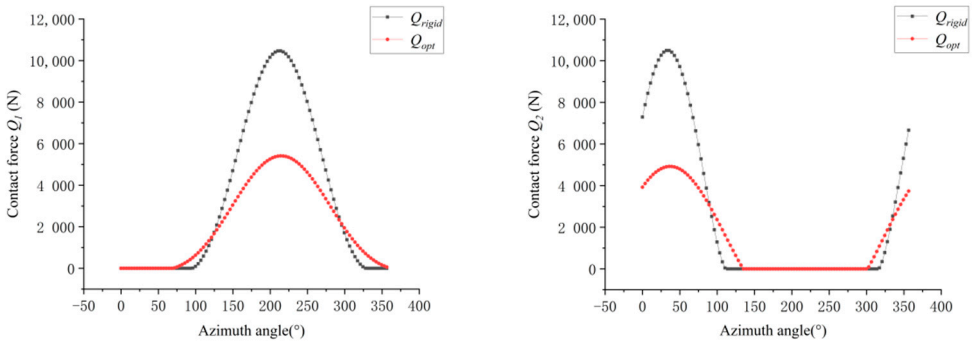


Figure 6. Contact force distribution before and after optimization: (**a**) contact force Q_1; and (**b**) contact force Q_2.

5.1.2. Deformation of Bearing Inner Raceway

Figure 7 shows the three-dimensional diagram of the optimized non-circular raceway and the circular raceway. Figures 7a and 7b represent the inner lower and upper raceways, respectively, where the red curve represents the traditional circular raceway, and the blue curve represents the actual shape of the optimized raceway. The three-dimensional diagram is projected to the bottom surface and the two sides respectively, and the radial and axial deformation of the non-circular raceway relative to the circular raceway can be clearly seen.

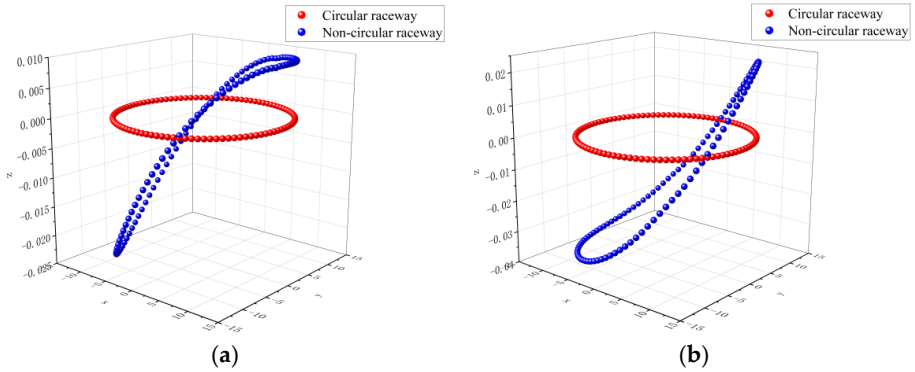


Figure 7. Three-dimensional diagram of bearing inner raceway: (**a**) inner lower raceway; and (**b**) inner upper raceway.

Figure 8 shows the comparison diagram of the non-circular raceway relative to the circular raceway after bearing load, where Figures 8a and 8b are the projections of the three-dimensional graphics in Figure 7a,b towards the bottom surface, respectively, indicating the radial deformation of the non-circular raceway relative to that of the circular raceway. Similarly, Figures 8c and 8d are three-dimensional diagrams. From the radial diagrams in Figure 8a,b, it can be seen that the inner lower raceway of the bearing deforms in the "left lower" direction relative to the circular raceway, and the inner upper raceway deforms in the "right upper" direction relative to the circular raceway. Comparing to Figure 6, it can be seen that the position where the non-circular and circular raceways deform is the very place where the contact force is different before and after optimization. When the contact force before optimization is greater than the contact force after optimization, the non-circular raceway displays "outward" deformation ($\Delta_{i,r} > 0$) relative to the circular raceway in the radial diagram; when the contact force before optimization is less than the optimized contact force, it displays as an "inward" deformation of the non-circular raceway relative to the circular raceway ($\Delta_{i,r} < 0$). The position where the maximum deformation of the non-circular raceway relative to the circular raceway occurs is the azimuth corresponding to the maximum contact force, which is 213.86° and 32.08°, respectively.

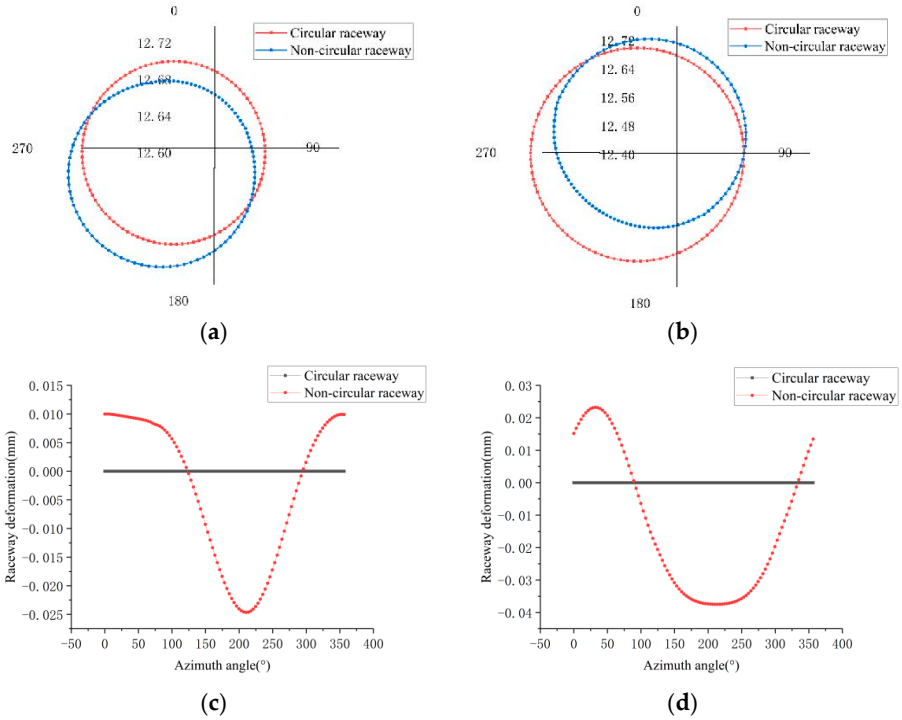


Figure 8. Bearing inner raceway of non-circular shape: (**a**) radial shape of inner lower raceway; (**b**) radial shape of inner upper raceway; (**c**) axial shape of inner lower raceway; and (**d**) axial shape of inner upper raceway.

It can be seen from the axial graph on Figure 8c,d that when the contact force before optimization is greater than the contact force after optimization, the deformation of the non-circular raceway relative to the circular raceway is different, namely: the inner and lower raceways undergo "downward" deformation ($\Delta_{i,a} < 0$), while an "upward" deformation ($\Delta_{i,a} > 0$) occurs in the inner upper raceway.

By contrast, when the contact force before optimization is less than the contact force after optimization, the inner and lower raceways have an "upward" deformation relative to the circular raceway ($\Delta_{i,a} < 0$); and a "downward" deformation ($\Delta_{i,a} > 0$) occurs in the inner and lower raceways. In the same way as in the radial diagram, the position where the maximum deformation occurs is also the position corresponding to the maximum contact force.

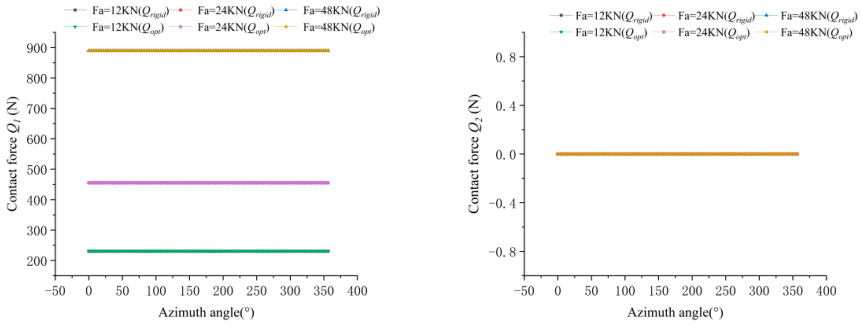
The above discussion reveals the optimal shape of the inner raceway of the bearing under the combined load in Table 2. Because the radial force of the wind turbine bearing is small in the working process, this paper mainly studies the influence of the axial force and overturning moment on the deformation of the bearing's inner raceway.

5.2. Pure Axial Force

5.2.1. Bearing Contact Load Distribution before and after Optimization

Figure 9a,b shows the bearing contact force distribution before and after optimization under pure axial force. Under the action of positive axial force, the inner ring of the bearing is offset upward from the outer ring, so the rolling body will be squeezed and loaded by the inner lower and outer upper raceways; while in the other direction, it will be separated from the raceway due to relaxation, that is, Q_1 and Q_2 as shown in Figure 2 show uniform load distribution. In addition, there is no substantial change in the contact form between the rolling body and raceway after optimization, and one side of the rolling body and raceway is still fully loaded while the other side is completely separated, so Q_2 is still 0, and the constraint condition of optimization is the static equilibrium equation of the bearing internal contact force and external load. Therefore, when the external load is fixed, Q_1 shows almost no change before and after optimization, and the change trend of Q_1 and the

external load is the same, that is, it increases with the increase in external load. When the axial load received is 12 KN, 24 KN and 48 KN, respectively, the corresponding contact force Q_1 is 231 N, 454N and 900 N, respectively.

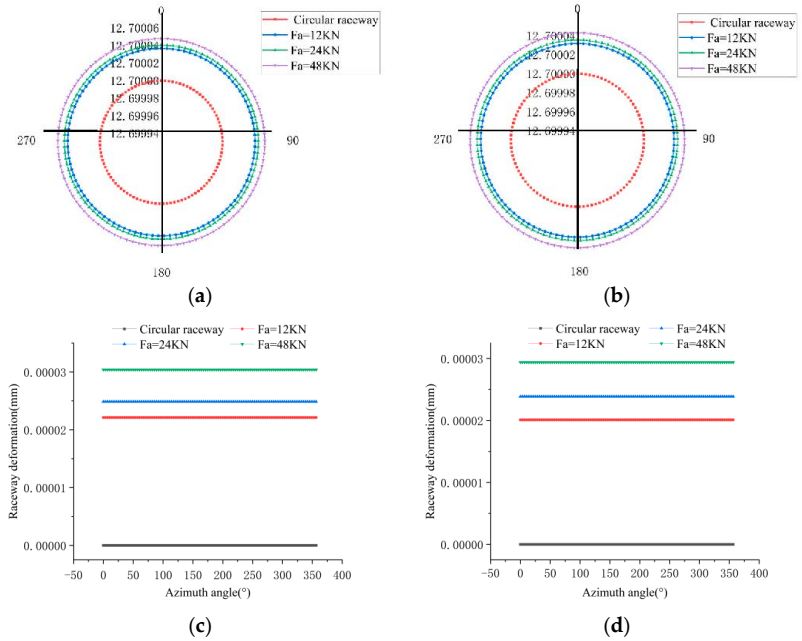


(**a**) (**b**)

Figure 9. Contact force distribution before and after optimization: (**a**) contact force Q_1; and (**b**) contact force Q_2.

5.2.2. Deformation of Bearing Inner Raceway

Figure 10 shows the deformation of a non-circular raceway relative to that of a circular raceway, where Figures 10a,b and 10c,d represent the radial and axial deformation, respectively. It can be seen from the figure that when subjected to pure axial load, the radial raceway of the two contact alignments corresponding to the maximum bearing life is still circular, and only the radius of the raceway is changed; moreover, the radial deformation of the bearing raceway is proportional to the magnitude of the axial load, that is, it increases with the increase in axial load (inner lower: 1.11×10^{-5}, inner upper: 1.1193×10^{-5}). Similar to the radial deformation, the axial shape of the optimal non-circular raceway of the optimized bearing is only a constant deformation compared with the circular raceway. The deformation increases with the increase in axial load (inner lower: 8.28×10^{-5}, inner upper: 9.3×10^{-6}), and the deformation is small.



(**a**) (**b**)

(**c**) (**d**)

Figure 10. Bearing inner raceway of non-circular shape: (**a**) radial shape of inner lower raceway; (**b**) radial shape of inner upper raceway; (**c**) axial shape of inner lower raceway; and (**d**) axial shape of inner upper raceway.

5.3. Pure Overturning Moment

5.3.1. Bearing Contact Load Distribution before and after Optimization

Figure 11a,b shows the bearing contact force distribution before and after optimization under the overturning moment. It can be seen from the diagram that before optimization, each rolling element of the bearing is basically in a normal contact, and the other is in a two-point contact state with normal separation. The load distribution of the rolling element is sinusoidal, and the load distribution of the rolling element is symmetrically distributed along the geometric center of the bearing. When the azimuth is $\psi = 181.8°$, the contact force Q_1 reaches the maximum 9209 N; when the azimuth is $\psi = 0°$, the contact force Q_2 reaches the maximum 9217 N. After optimization, the contact force in the rolling body has changed significantly compared with that before optimization. The maximum contact force of Q_1 and Q_2 is 4005 N and 4007 N, respectively, which is respectively 5205 N and 5210 N lower than that before optimization. The azimuth of the maximum contact force has not changed. It can be seen that the optimized increase in the bearing area of the rolling element, making the load distribution more uniform, effectively improves the bearing capacity.

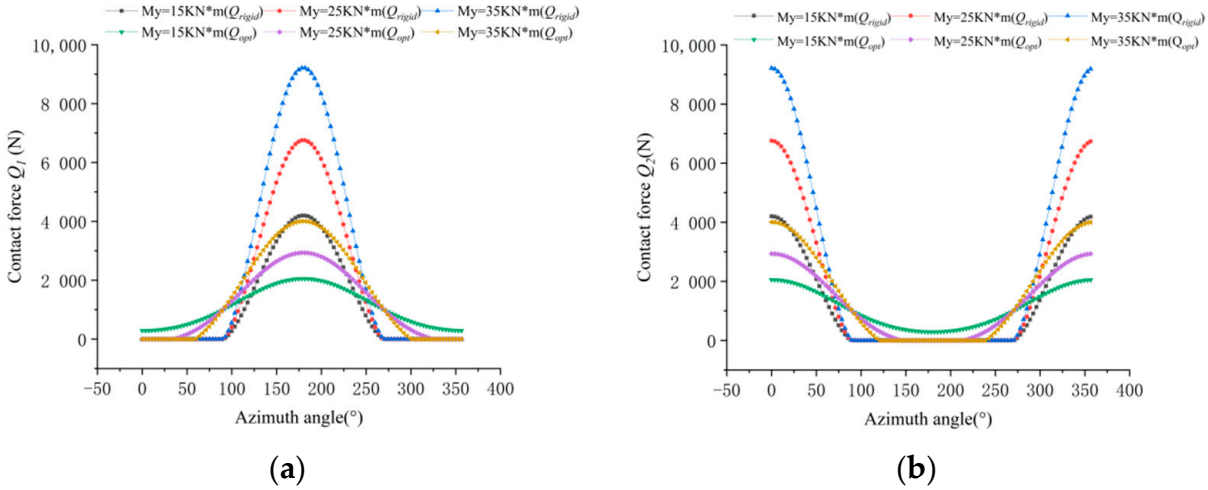


Figure 11. Contact force distribution before and after optimization: (**a**) contact force Q_1; and (**b**) contact force Q_2.

5.3.2. Deformation of Bearing Inner Raceway

Figure 12 shows the deformation of a non-circular raceway relative to a circular raceway, where Figures 12a,b and 12c,d represent the radial and axial deformation, respectively. Compared with Figure 11, it can be seen that when the contact force before optimization is greater than the optimized contact force, in the radial diagram, the deformation of the non-circular raceway is "outward" relative to that of the circular raceway ($\Delta_{i,r} > 0$), and the deformation trend of the deformation and the contact force is the same, which increase with the increase in overturning moment (inner lower: 1.43×10^{-2}, inner upper: 1.429×10^{-2}).

When the contact force before optimization is less than that after optimization, the radial diagram shows that the non-circular raceway deforms "inward" relative to the circular raceway ($\Delta_{i,r} < 0$), and the deformation also increases with the increase in overturning moment (inner lower: 1.44×10^{-2}, inner upper: 1.193×10^{-2}).

From the axial graph Figure 12c,d, it can be seen that when the contact force before optimization is greater than the optimized contact force, the inner and lower raceways have a "downward" deformation relative to the circular raceway ($\Delta_{i,a} < 0$), and the inner upper raceway has an "upward" deformation relative to the circular raceway ($\Delta_{i,a} > 0$). The deformation also increases with the increase in overturning moment (inner lower: 1.322×10^{-2}, inner upper: 1.991×10^{-2}).

When the contact force before optimization is less than the contact force after optimization, the inner and lower raceways have "upward" deformation ($\Delta_{i,a} > 0$) relative to

the circular raceway, and the inner and upper raceways have "downward" deformation ($\Delta_{i,a} < 0$) relative to the circular raceway. The deformation also increases with the increase in overturning moment (inner lower: 1.322×10^{-4}, inner upper: 1.991×10^{-3}).

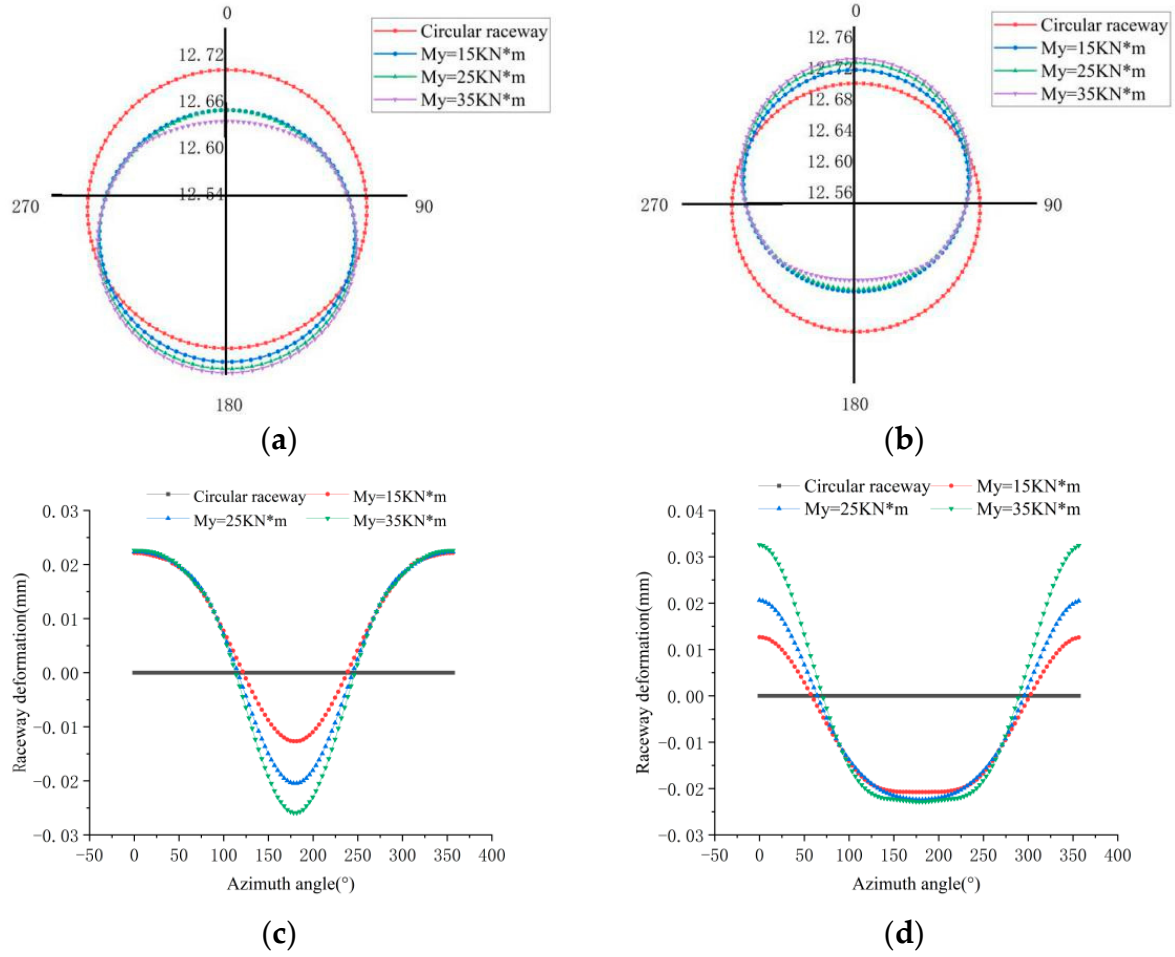


Figure 12. Bearing inner raceway of non-circular shape: (**a**) radial shape of inner lower raceway; (**b**) radial shape of inner upper raceway; (**c**) axial shape of inner lower raceway; and (**d**) axial shape of inner upper raceway.

5.4. Combined Action of Axial Load and Overturning Moment

5.4.1. Bearing Contact Load Distribution before and after Optimization

Figure 13a,b shows the bearing contact force distribution before and after optimization under the combined action of axial force and overturning moment. As can be seen from the figure, due to the overturning moment of the bearing compared to its axial load, its value is very large. Thus, the distribution of the contact force inside the bearing and the distribution of the contact force under the action of pure overturning moment is basically the same—namely, the symmetrical load distribution in accordance with the sine law—and the distribution of contact force is more compact. Before optimization, when the azimuth is $\psi = 181.8°$, the contact force Q_1 reaches the maximum; when the azimuth is $\psi = 0°$, the contact force Q_2 reaches the maximum. For a certain overturning moment, the maximum contact force in the bearing will decrease with the increase in axial load, and will increase the bearing area. Meanwhile, the maximum contact force corresponding to the azimuth angle did not change, but the bearing contact force was significantly reduced and the rolling element bearing area increased, effectively improving the bearing capacity of the ball bearing.

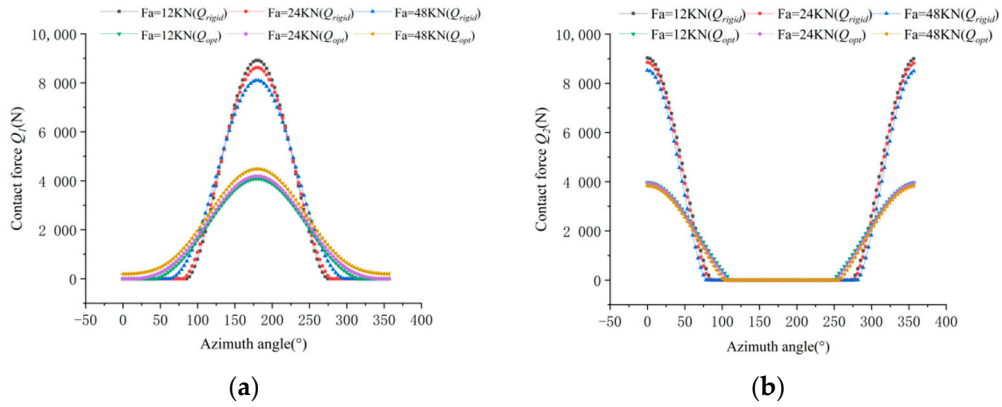


Figure 13. Contact force distribution before and after optimization: (**a**) contact force Q_1; and (**b**) contact force Q_2.

5.4.2. Deformation of Bearing Inner Raceway

Figure 14 shows the deformation of a non-circular raceway relative to a circular raceway, where Figures 14a,b and 14c,d represent the radial and axial deformation, respectively. It can be seen from the figure that under the combined action of axial load and overturning moment, the shape of the non-circular raceway is roughly the same as that under pure overturning moment—that is, the deformation of the raceway also occurs at different positions of contact force before and after optimization.

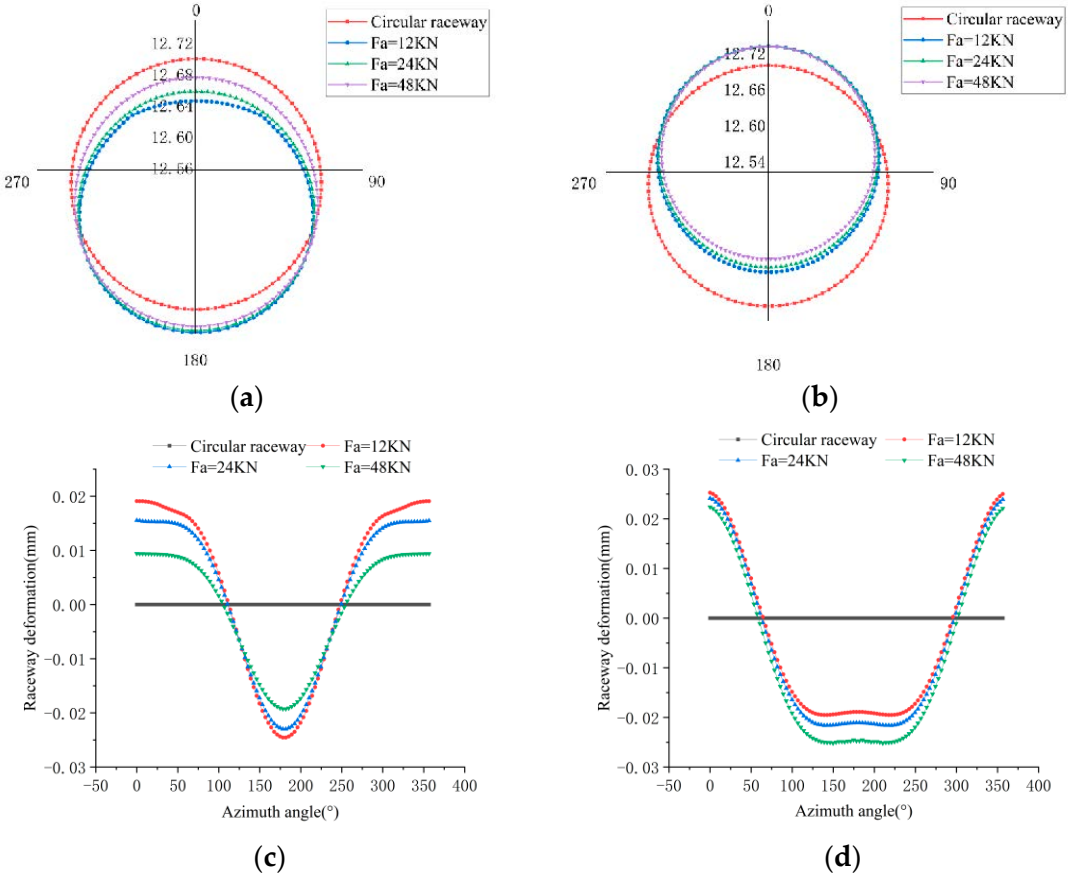


Figure 14. Bearing inner raceway of non-circular shape: (**a**) radial shape of inner lower raceway; (**b**) radial shape of inner upper raceway; (**c**) axial shape of inner lower raceway; and (**d**) axial shape of inner upper raceway.

The difference in this case is that when the contact force before optimization is greater than the optimized contact force, the maximum deformation of the inner and lower raceways decreases with the increase in axial load (radial: -3.1544×10^{-2}, axial: -5.22×10^{-3}), and the deformation of the inner and upper raceways decreases with the increase in axial load (radial: -2.1764×10^{-5}, axial: -1.688×10^{-3}).

When the contact force before optimization is less than the contact force after optimization, the axial deformation of the inner raceway will increase with the increase in axial load (increment: 8.852×10^{-3}).

6. Summary and Conclusions

Based on the Hertz contact theory, the equilibrium equation of the bearing under the action of external load and internal contact load is established by using the vector method, and the rated life of the single-row four-point contact ball bearing is calculated. The optimal load distribution inside the bearing is optimized by taking the maximum bearing life as the objective function. The optimal non-circular deformation of the inner ring corresponding to the maximum bearing life is studied, and the following conclusions are drawn.

1. Under the influence of pure axial load, the two contact pairs of the bearing correspond to full load and full separation respectively. There is no obvious change in the contact force inside the bearing before and after optimization. The deformation of the optimal raceway is almost 0 compared with that of the traditional circular raceway. At this time, the circular raceway is the optimal raceway shape corresponding to the maximum life.
2. Under the influence of pure overturning moment, the contact force Q_1 and Q_2 are sinusoidally distributed. The position where the raceway deformation occurs is the position where the contact force before and after optimization is different. The deformation of the raceway is proportional to the change in overturning moment, that is, it increases with the increase in overturning moment.
3. Under the combined action of axial load and overturning moment, the distribution trend of the internal contact force of the bearing is roughly the same as that under the action of pure overturning moment, that is, it obeys the regular sinusoidal change. At this time, the corresponding raceway shape is roughly the same as that under the action of pure overturning moment, and only the amplitude of the raceway shape variable is changed.

In this paper, a calculation method for a non-circular optimal raceway of a four-point contact slewing ball bearing is mainly proposed. This method is also applicable to other bearings. In subsequent research, the actual processing will be carried out based on the pre-deformation measurements from the current research, and the feasibility of the method will be verified by experiments.

Author Contributions: Y.Z. conceived and designed the analysis, collected and analyzed data, and wrote and revised the paper; G.C. conceived and designed the analysis and revised the paper; W.Z. provided guidance on the numerical simulation software; Y.D. verified the results. All authors have read and agreed to the published version of the manuscript.

Funding: This research received no external funding.

Institutional Review Board Statement: Not applicable.

Informed Consent Statement: Not applicable.

Data Availability Statement: Not applicable.

Acknowledgments: The authors thank the anonymous reviewers, who provided valuable suggestions that improved the manuscript.

Conflicts of Interest: The authors declare no conflict of interest.

Nomenclature

O	centre of the ball
ou, od	inner upper/lower raceway curvature center
iu, id	outer upper/lower raceway curvature center
iu'	outer upper curvature center after optimization
O_0	centre of the bearing
$o_{i,r}$	radial distance between curvature center of inner raceway and ball center in the case of a bearing without clearance
$o_{i,a}$	axial distance between inner (outer) upper raceway center and ball center in the case of a bearing without clearance
$o_{o,r}$	radial distance between curvature center of outer raceway and ball center in the case of a bearing without clearance
$o_{o,a}$	axial distance between inner (outer) lower raceway center and ball center in the case of a bearing without clearance
D_w	rolling element (ball) diameter
D_{pw}	bearing pitch circle diameter
g_0	clearance
ψ	angle defining circumferential position of the rolling element (ball)
α_0	nominal contact angle
C	contact point
r	raceway curvature radius
f	raceway curvature coefficient
T	transformation matrix
u, v, w	translations of the bearing ring along axes x, y and z
φ_x, φ_y	rotations of the bearing ring around axes x and y
x, y, z	axes of Cartesian coordinate system
x'	axis in the radial direction of the bearing defining vertical plane at angle ψ
Z	number of rolling elements (ball)
δ	relative approach of the two opposite raceways
δ'	relative approach of the two opposite raceways after optimization
Δ	displacement of the centre of the raceway
$\vec{r}$	position vector
$\vec{e}$	unit vector of the contact force
K	contact stiffness
$\vec{F}, \vec{M}$	vectors of forces/tilting moments acting on the bearing
F_x, F_y, F_z	scalars of radial force/axial force acting on the bearing
M_x, M_y	scalar of overturning moment acting on bearing
Q	contact force acting on the raceway in scalar form
Q'	contact force acting on the raceway in scalar form after optimization
$Q_{ci(o)j}$	basic rated dynamic load bearing
λ, η	correction coefficient of ball bearing
L_{10}	rated life of bearings
γ	$D_w \cos \alpha_0 \Big/ D_{pw}$
Subscripts	
i, o	inner/outer ring
j	subsequent number of contact force
ψ	value of parameter at azimuth (angle) ψ

References

1. Niu, R.J.; Xun, J.C.; Shao, X.H.; Deng, S.E. Mechanical Performance Analysis of Double row Asymmetric Four point Contact Ball Turntable Bearings. *J. Mech. Eng. Chin. Ed.* **2018**, *54*, 177–186. [CrossRef]
2. Rui, X.M.; Zheng, H.; Huang, H.R. Research on load distribution of wind turbine pitch bearing. *Proc. Chin. Soc. Electrical. Eng.* **2013**, *33*, 80–87+2.
3. Yang, X.B.; Zhang, T.; He, L.Z.; Bu, Z.J.; Liu, M.Z.; Li, M. Study on friction torque characteristics of large double row four point contact ball bearing. *Acta Energ. Sol. Sin.* **2021**, *42*, 356–363.

4. Zhang, L.Y.; Wang, Y.S.; Yuan, Q.Q.; Ji, Y.G. Influence of Load and Geometry Parameter on Load Distribution of a Single-row Four-point-contact Ball Slewing Bearing. *J. Mech. Tran.* **2013**, *37*, 27–29+101.
5. Wang, Y.S.; Yuan, Q.Q.; Cao, J.W.; Li, P.; Li, Y. Research on Static Load-carrying Capacity of Large Size Double Row Four-point Contact Ball Bearings. *J. Mech. Eng. Chin. Ed.* **2014**, *50*, 65–70. [CrossRef]
6. Robert, K.; Ivan, P. Numerical determination of carrying capacity of large rolling bearings. *J. Mater. Sci. Technol.* **2004**, *155*, 1696–1703.
7. Du, J.; Dai, X.L.; Yang, X.G.; Jin, X.; Zhou, Y.P.; Zhang, L. Influence pf bolt pretension on load distribution of large type double row four-point-contact ball bearing. *Acta Energ. Sol. Sin.* **2017**, *38*, 2645–2651.
8. Kabus, S.; Pedersen, C.B.W. Optimal Bearing Housing Designing Using Topology Optimization. *J. Tribol. April.* **2012**, *134*, 021102. [CrossRef]
9. Hou, G.Z. *Study on the Effect of Non-Uniform Preload of Bolt and Topology Optimization of Supporting Structure on the Life od Slewing Bearing*; Kunming University of Science and technology: Kunming, China, 2018; p. 53.
10. Mao, Y.Z.; Wang, L.Q.; Gu, L. Analysis of the influence of negative clearance on the dynamic performance of high speed temperature thin walled cylindrical roller bearings. *J. Aerosp. Power* **2016**, *31*, 2795–2800.
11. Yue, J.D.; Deng, S.E.; Ni, S.J.; Li, L.; Yang, H. Calculation of friction moment of thin walled four point contact ball bearing with negative clearance under no load. *Bearing* **2014**, *3*, 022.
12. Xu, S.R.; Yang, Y.Z.; Bai, Y.G.; Wang, Y.S.; Deng, S.E. Quasi-static analysis of super large negative clearance four point contact ball bearing. *Bearing* **2009**, *9*, 001.
13. Li, Y.F.; Wu, Z.Y.; Lu, B.H.; Zhao, G.Y.; Sun, L.M. Influence of Clearance on Load Distribution of Single Row Four-point Contact Ball Slewing Bearings. *J. Mech. Tran.* **2010**, *34*, 56–58.
14. Ambrożkiewicz, B.; Syta, A.; Gassner, A.; Georgiadis, A.; Litak, G.; Meier, N. The influence of the radial internal clearance on the dynamic response of self-aligning ball bearings. *Mech. Syst. Signal Process.* **2022**, *171*, 108954. [CrossRef]
15. Chudzik, A.; Warda, B. Effect of radial internal clearance on the fatigue life of the radial cylindrical roller bearing. *Eksploat. Niezawodn.* **2019**, *21*, 211–219. [CrossRef]
16. Tomović, R. Load Calculation of the Most Loaded Rolling Element for a Rolling Bearing with Internal Radial Clearance. *Appl. Sci.* **2020**, *10*, 6934. [CrossRef]
17. Chen, G.C.; Jia, P.; He, J.Q. Effects of geometric parameters on static load capacity of a double-row four-point contact ball bearing. *J. Mech. Sci. Technol.* **2013**, *27*, 1053–1061. [CrossRef]
18. Glodez, S.; Potocnik, R.; Flasker, J. Comoutational model for calculation of static capacity and lifetime of large slewing bearings's raceway. *Mech. Mach. Theory* **2012**, *4*, 16–30. [CrossRef]
19. Rok, P.; Goencz, P.; Glodez, S. Static capacity of a large double row slewing ball bearing with predefined irregular geometry. *Mech. Mach. Theory* **2013**, *64*, 67–79.
20. Wang, Q.Y.; Zhao, Y.L.; Wang, M.Z. Analysis of Contact Stress Distribution between Rolling Element and Variable Diameter Raceway of Cageless Bearing. *J. Appl. Sci.* **2022**, *12*, 5764. [CrossRef]
21. Luo, T.Y.; Luo, J.W. Influence of raceway ovality on bearing fatigue life. *Bearing* **2013**, *12*, 003.
22. He, P.P. Study on the influence of raceway ovalization on contact characteristics and fatigue life of high speed angular contact ball bearings. *J. Mach. T. Hydr.* **2020**, *48*, 195–201.
23. Li, Y.F.; Jiang, D. Finite Element Analysis of Wind Power Pitch Bearing Considering Installation Structure. *Acta Energ. Sol. Sin.* **2019**, *40*, 2021–2027.
24. Liu, Y.; Li, Y.C.; Liu, J.; Wang, H. Study on Load Capacity of Single Row Four Point Contact Ball Slewing Bearings. *Bearing* **2018**, *12*, 009.
25. Yang, X.Q. *Contact Mechanics Theory and Rolling Bearing Design Analysis*; Huazhong University of Science & Technology Press: Wuhan, China, 2018; Volume 4.
26. Wang, Y.S.; Yuan, Q.Q. Influence of Negative Clearance on Load Distributions of Large-size Double Row Four-point-contact Ball Bearings. *J. Mech. Eng. Chin. Ed.* **2012**, *48*, 110–115. [CrossRef]
27. Lundberg, G.; Palmgren, A. Dynamic Capacity of Rolling Bearings. *J. Appl. Mech.* **1949**, *16*, 165–172. [CrossRef]
28. Yuan, Q.Q.; Wang, Y.S. Fatigue life calculation of pitch bearing. *Bearing* **2012**, *12*, 005.
29. Wan, C.S. Analysis method of rolling bearing. *China Mach. Press* **1987**, *3*.